Detection and Certification of Faint Streaks in Astronomical Images

Vojtěch Cvrček and Radim Šára[a]
Department of Cybernetics, Czech Technical University in Prague, Czech Republic

Keywords: Space Debris, Object Detection, Bayesian Model Selection, Image Analysis and Understanding.

Abstract: Fast-moving celestial objects, like near-Earth objects (NEOs), orbiting space debris, or meteors, appear as streaks superimposed over the star background in images taken by an optical telescope at long exposures. As the apparent magnitude of the object increases (the object becomes fainter), its detection becomes progressively harder. We discuss a statistical procedure that makes a binary decision on the presence/absence of a streak in the image which is called *streak certification*. The certification is based purely on a single input image and a public star catalog, using a minimalistic statistical model. Certification accuracy greater than 90% for streaks of arbitrary orientation, longer than 500 pixels, and the signal-to-background log-ratio is better than -10 dB is achieved on the same dataset as in an earlier similar method, whose performance is thus exceeded, especially for close-to-horizontal streaks. We also show that the certification decision indicates detection failure well.

1 INTRODUCTION

With the rise of spatial traffic around Earth, Space Situational Awareness (SSA) gradually became an established field (Bobrinsky and Del Monte, 2010). It brought the need for object detection, most importantly space debris, which are unwanted man-made passive objects of various sizes orbiting Earth. Their orbital parameters may be difficult to predict, due to random influences, like solar wind, etc. Better detection methods lead to safety increase in the Earth orbit by improving collision prevention. Detection of other near-Earth objects is also of interest (Yanagisawa et al., 2005). Besides radar observations, optical observations are widely considered a suitable modality for detection. Any automatic cataloging process of a large number of such objects requires a statistical assessment of detection significance.

We consider optical observations of such objects. In a typical setup, long-exposure images are taken in a sequential manner. Objects of interest appear as streaks in these images, an example is shown in Fig. 1. A streak is a line segment parameterized by position, length, angular orientation, amplitude (or brightness), and cross-sectional profile (width). The streak, oriented approximately in a lower-left to upper-right direction in Fig. 1 is not very difficult to detect although it may not be visible to inexperienced reader at first sight.

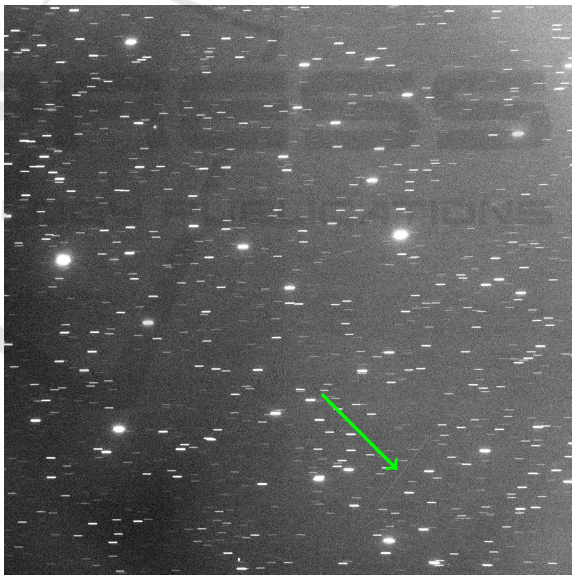

Figure 1: Input image, the green arrow points to the streak ($-38°$, SBR = -5.26 dB). Best viewed close-up, in PDF.

It is common that few images in an observation sequence contain a streak. These images are hard to select manually. We therefore consider the following task: Given a single optical image like the one in Fig. 1, we wish to decide if the image contains a streak or not and determine the parameters of the streak if it does. We discuss a formal framework for the statistical decision part of the task that has been called *certification* in (Sara and Cvrcek, 2017).

[a] https://orcid.org/0000-0002-2032-5764

Cvrček, V. and Šára, R.
Detection and Certification of Faint Streaks in Astronomical Images.
DOI: 10.5220/0007399804980509
In *Proceedings of the 14th International Joint Conference on Computer Vision, Imaging and Computer Graphics Theory and Applications (VISIGRAPP 2019)*, pages 498-509
ISBN: 978-989-758-354-4

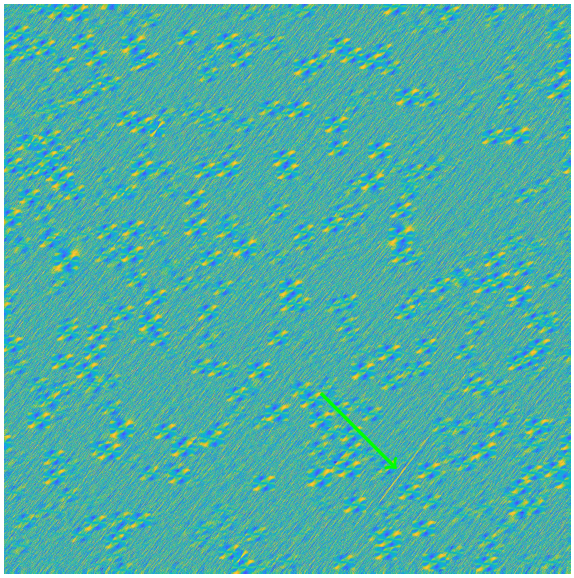

Figure 2: Filter response ($\phi = -38°$) to the image from Fig. 1, stars are not suppressed (Sara and Cvrcek, 2017).

Figure 3: Filter response ($\phi = -38°$) to the image from Fig. 1 with star suppression.

In that view, the parameter inference (detection) is a secondary task. The certification (or detection) becomes progressively more difficult with decreasing signal-to-background ratio (SBR) and decreasing streak length. In addition, in case of a passive telescope (without sidereal tracking, as is the case in Fig. 1) the certification and detection problems are not equally difficult for all orientation angles because stars appear as short streaks as well.

1.1 Related Work

The streak detection problem and its variations has been studied for more than two decades (Leu, 1992). Known methods can be divided to two broad categories: Single-frame methods that work with a single image (Ciurte and Danescu, 2014; Virtanen et al., 2016; Tagawa et al., 2016) and multiframe methods that track the object (Yanagisawa et al., 2008; Sun et al., 2015; Uetsuhara and Ikoma, 2014; Yanagisawa and Kurosaki, 2012; Šára et al., 2013) and/or use streak-free images for background subtraction (Leu, 1992; Gural et al., 2005).

A long streak appears if the observed object moves fast and appears in just a single frame. Some authors also consider slowly moving objects that are observed repeatedly over the course of several frames (Leu, 1992; Uetsuhara and Ikoma, 2014). The 'streaks' in a single frame are then very short. To achieve reliable detection, it must be coupled with tracking. We do not consider such approaches in this paper and focus on long streaks (at least 50 pixels, say).

Simple detection methods use matched filters (Gural et al., 2005). Each parameter vector defines a convolutional filter that is applied to the image. Parameters include streak shape and pose. Detection is done by non-maximum suppression with thresholding. The threshold can be learned (Schildknecht et al., 2015). The matched-filter approaches perform an exhaustive search, possibly with some speedup heuristics (Schildknecht et al., 2015). In these methods there is a tradeoff between parameter space discretization step and detection accuracy.

A well-known method in the class of single-frame long-streak detection is based on image column medians (Yanagisawa and Nakajima, 2005): Even a faint vertical streak of sufficient length can be detected by computing columnwise image medians and thresholding the result. This gives the column position. The streak is then localized within that column. Streaks in other orientations are detected with the help of image rotation. This method requires a very fine quantization of angular space (around 360 discrete angles in (Yanagisawa and Nakajima, 2005) for region 700×700 pixels, bigger images require even finer quantization). On the other hand, the algorithm is easily parallelizable which makes the method useful. The method is robust: Bright stars and noise have low impact on the median. A less robust but computationally efficient methods are based on Radon transform (Zimmer et al., 2013). These methods share the limitation due to angular discretization.

Recent single-frame methods employ a bottom-up procedure of salient pixel detection, followed by per-

ceptual grouping (Virtanen et al., 2016). The method does not distinguish short/long streaks. It achieves state of the art performance on a proprietary dataset.

Some recent approaches try avoiding early decisions, acknowledge the statistical nature of the problem and employ a formal classification/hypothesis testing. An interesting method in this class is (Kolessa, 2013). The method first considers local image structure and categorizes it to several classes (background/star/streak tracklet). Streaks are then detected by concatenating streak tracklets. Another statistically sound method is presented in (Dawson et al., 2016). The methods maximizes image likelihood by streak parameter space search.

A recent statistical method distinguishes two phases of the problem: Detection and certification (Sara and Cvrcek, 2017). Detection infers streak parameters in the Maximum a Posteriori (MAP) sense, assuming there is a streak in the image. Certification is a decision if the image contains a streak. These two tasks are coupled in what the paper calls Multi-Level Bayesian Inference (MLBI). The certification is done by Bayesian model selection. Two statistical models are considered: (1) M_1: image contains a streak, and (2) M_0: image does not contain a streak. Model selection is based on computing posterior marginals for the two models and comparing their value. The nice property of the method is that the marginals can be computed exactly with a low-order polynomial algorithm (Sara and Cvrcek, 2017). The method achieved state-of-the art performance in a restricted streak angle range: The presence of axis-aligned CCD chip artefacts (vertical, horizontal) and star streaks (horizontal) resulted in false-positive certification for these angles, hence the algorithm worked with these angles excluded.

The present paper aims to develop the method from (Sara and Cvrcek, 2017) further. The underlying principles are the same. We removed the angular limitation of the previous method by background simulation and subtraction in feature space, as detailed in Sec. 2.1. This led to significant performance improvement and pushed the performance boundary towards very faint streak certification, as shown in Sec. 4. The main focus of this paper is on certification. We nevertheless describe the detection procedure and verify consistency of the proposed certification and ground-truth based detection rejection using a threshold on location error of the detection.

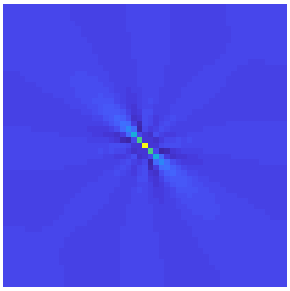

Figure 4: Example of an oriented streak template. The template's orientation is $\phi = -45^\circ$.

2 METHOD

Each pixel $x_{i,j}$ (we might drop the indices i, j in subsequent text) in the image X is represented by a feature vector $\mathbf{f}(i, j)$, of dimension d ($d = 5$). The feature vector $\mathbf{f}(i, j)$ represents a local region w.r.t. to a certain family of templates (Marchant and Jackway, 2012a). A streak segment template in Fig. 4 is represented by a vector $\mathbf{t}$ of size d that can be rotated in $O(d)$. Similarity between region represented by $\mathbf{f}$ and $\mathbf{t}$ rotated by ϕ is then computed in $O(d)$ time. This is faster than rotating the original streak template in Fig. 4 and convolving with the input image for each angle. Details how to construct $\mathbf{f}$ and $\mathbf{t}$ are provided in (Marchant and Jackway, 2012a). Additional details for computing similarity in an identical setting can be found in (Sara and Cvrcek, 2017).

Some image objects resemble streaks (stars in a passive telescope, CCD imager segment boundaries), thus inducing high response (although they belong to the background). This often leads to false positives. The paper (Sara and Cvrcek, 2017) deals with this problem by prohibiting problematic angles. Thus, the angular degree interval $[-90,-73.5] \cup [-5.5,5.5] \cup [73.5,90]$ was excluded in (Sara and Cvrcek, 2017). But then a streak with an orientation in that interval leads to a false negative. In this paper, we wish to extend the solution to every orientation of a streak. To do this (1) we construct simulated background in Sec. 2.1, and (2) we will show how to modify the feature vectors to compensate background artefacts in Sec. 2.1.

2.1 Normalized Image Representation

Our objects of interest are celestial objects that produce streaks in long-exposure images. If the object was not present, we would observe what we call the *background image*. As discussed above, the background image contains structures (stars and

image artefacts) that lead to false positive certifications/detections. In this paper, we will show how to suppress these artefacts by modifying the feature representation of the image.

One can either obtain stars by detection, directly in the input image (Schildknecht et al., 2015), or from registering the image against a star catalog (Zimmer et al., 2013). With the first approach, we risk detecting a streak as a star, or ignoring a star altogether. Rather than a truth we see the star catalog as an *independent but imperfect source of information*. We should note that automatically constructed catalogs are incomplete in objects of large apparent magnitudes but up to the limiting magnitude of a typical telescope it can be considered complete.

With a catalog or without, the usual approach is to mask the stars out (Schildknecht et al., 2015), thus loosing some data. We will avoid such early decisions by using the star catalog and some characteristics of the input image to simulate the background of the input image in the space of aforementioned features.

Assuming our background simulation was perfect, then due to additivity, we could get the pure streak image by simply subtracting the background image from the input image. Unfortunately, simulating the background in sufficient quality is very difficult since the image is influenced by many physical phenomena (consider e.g. image saturation or blooming, or thin clouds in the upper atmosphere partly dimming the stars and reflecting stray light from the Earth). We found that if the subtraction is done in the space of normalized image features, the idea works with even a very coarse simulation. Moreover, the simulation tends to work very well for bright stars that tend to attract the detector/skew certification. These kinds of objects are causing most of typical false positives in previous methods (Zimmer et al., 2013).

Background simulation is done as follows. Each star in the catalog has an apparent magnitude M. Magnitude is not directly measurable in the image. We therefore recover the star magnitude-to-image flux mapping. The images are first registered to the catalog by the method used in (Šára et al., 2013). For each catalogued star and the given image exposure time, an elongated star image region S is defined. Flux F_m of the star in the image is computed by integrating image values over S. This way we collect (flux, magnitude) samples. Apparent magnitudes M from the star catalog are matched to flux F_m by robustly fitting a piece-wise linear function to this data. Catalogued stars are simulated by rendering a line segment of length l proportional to exposure time and amplitude proportional F_m/l. The resulting simulated image is then convolved with a Gaussian point spread function. Its σ parameter was learned from star samples.

Finally, random Gaussian noise with zero mean was added. The standard deviation of the noise was learned as the sample standard deviation of the input image, with image regions containing stars masked out (solely) for this purpose.

Let $\mathbf{f}_{\mathrm{im}}(i,j)$ be steerable feature vector computed at an input image pixel (i,j) and $\mathbf{f}_{\mathrm{sim}}(i,j)$ be feature vector computed at the corresponding pixel of the simulated image. The features are spherical quadrature filter responses (Marchant and Jackway, 2012b) with the zero-order filter excluded, see (Sara and Cvrcek, 2017) and references therein for details. The exclusion helps suppress additive artefacts. We then normalize the vectors to suppress scaling artefacts and then subtract them:

$$\mathbf{f}_{\mathrm{res}}(i,j) = \frac{\mathbf{f}_{\mathrm{im}}(i,j)}{\|\mathbf{f}_{\mathrm{im}}(i,j)\|} - \frac{\mathbf{f}_{\mathrm{sim}}(i,j)}{\|\mathbf{f}_{\mathrm{sim}}(i,j)\|}, \qquad (1)$$

where $\|\cdot\|$ is the Euclidean norm.

The effect of this simulated background subtraction in feature space can be seen in Fig. 2 and 3. We found that this feature modification dramatically contributes to the overall success of the certification/detection method as the experimental results in Sec. 3 show.

2.2 Model

We study two events. In the first event, there is no statistically significant streak with an orientation ϕ in an image X. We denote the Bayesian model for the no-streak event as $p_0(X,\phi)$. The second event is a presence of a single statistically significant streak with an orientation ϕ and parameters θ (eg. starting and ending position) in the image X. We denote the Bayesian model for the single-streak event as $p_1(X,\phi,\theta)$.

We lift the image 2D grid to 3D grid by assuming a discrete set of angles Φ. The lifted image element value $x_{\phi,i,j}$ is then the similarity value between the streak segment template of the orientation ϕ and image at the pixel position (i,j). We denote similarities for a particular orientation $X_\phi = \{x_{\phi,i,j} \mid (i,j) \in \mathcal{X}\}$, where $\mathcal{X}$ is the image domain. The complete 3D stack is $X_\Phi = \{X_\phi \mid \phi \in \Phi\}$.

The quantization Φ stems from the fact that streaks are not infinitely thin. The orientation ϕ is then a discrete random variable. The motivation for lifting data to 3D is that we need to express the fact that a possible streak can appear in just a single orientation. This is a substantial modification of the original model (Sara and Cvrcek, 2017). In summary, we assume that $p_0(X,\phi+\Delta\phi) \approx \hat{p}_0(X_\phi)$ and $p_1(X,\phi+\Delta\phi,\theta) \approx$

$\hat{p}_1(X_\phi, \phi, \theta)$, when ϕ is fixed and $|\Delta\phi|$ is sufficiently small.

First, we develop the two models $\hat{p}_0(X_\phi)$ and $\hat{p}_1(X_\phi, \phi, \theta)$. Then, we use the models to (1) find the best streak in the image (detection), and (2) decide about the statistical significance of the founded streak (certification).

2.2.1 No-streak Model Distribution

We first construct distribution $p_b(x_{\phi,i,j}; \zeta_b(\phi))$ with hyper-parameters $\zeta_b(\phi)$ that a single-pixel similarity originates from a background. Given a fixed orientation $\phi \in \Phi$ and the input image, we learn the distribution p_b as a normalized histogram with hyper-parameters $\zeta_b(\phi)$. The histogram is constructed from all steered similarity responses $x_{\phi,i,j}$ collected over the image domain for a given angle ϕ. The effect of a possible streak in the image is negligible in the histogram due to its small support in the image. An example of the background pixel-wise distribution p_b is the blue distribution in Fig. 5.

We assume pixel-wise independence and we construct following joint image model distribution for particular orientation ϕ

$$\hat{p}_0(X_\phi) = \prod_{i,j \in \mathcal{X}} p_b(x_{\phi,i,j}; \zeta_b(\phi)). \quad (2)$$

where X_ϕ is the similarity map.

The distribution that the image is a background $p_0(X) \approx \hat{p}_0(X_\Phi)$ is the joint distribution that every 3D pixel is part of the background

$$\hat{p}_0(X_\Phi) = \hat{p}_0(X_{\phi_1}, .., X_{\phi_k}) = \prod_{\phi \in \Phi} \hat{p}_0(X_\phi) = \prod_{\phi \in \Phi} \prod_{i,j \in \mathcal{X}_\phi} p_b(x_{\phi,i,j}; \zeta_b(\phi)). \quad (3)$$

The background model is hence parameterless.

2.2.2 Streak Model Distribution

We first construct distribution that a single-pixel similarity originates from a streak $p_1(x_{\phi,i,j}; \zeta_1(\phi))$, which is an analogue to $p_b(x_{\phi,i,j}; \zeta_b(\phi))$ in (3). This is done in a way similar to (Sara and Cvrcek, 2017). It is assumed that a streak adds an unknown additive quantity to similarity $x_{\phi,i,j}$. This is approximately true even after normalization in (1) for small streak amplitudes. Since the amplitude of the streak is unknown, we assume a random variable of uniform distribution $p_u(x; a, b)$, where x is a similarity shift and (a, b) is a sufficiently wide shifts interval. The $p_1(x_{\phi,i,j}; \zeta_1(\phi))$ is then given by

$$p_1 = p_b * p_u. \quad (4)$$

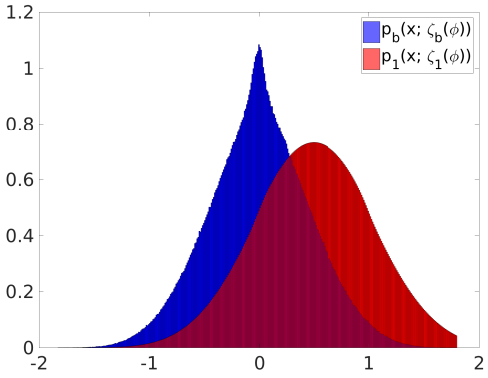

Figure 5: Pixelwise distributions $p_b(x_{\phi,i,j}; \zeta_b(\phi))$ and $p_1(x_{\phi,i,j}; \zeta_1(\phi))$ for $\phi = -38°$.

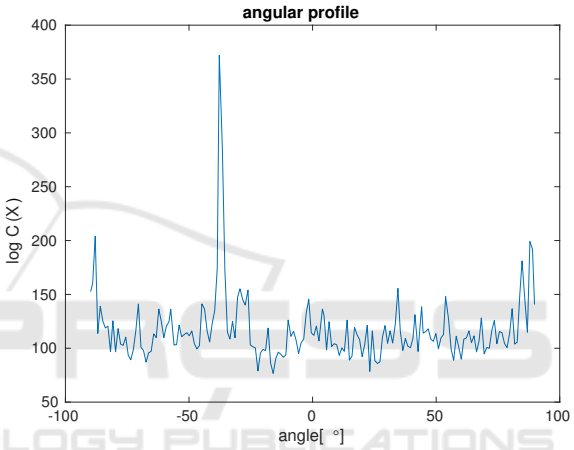

Figure 6: Angular profile of the input image in Fig. 1, with a prominent peak corresponding to the streak orientation angle.

Where $*$ represents convolution and $\zeta_1(\phi)$ are hyper-parameters of a normalized histogram. A typical result is the red distribution in Fig. 5.

Suppose we work at a given angle ϕ. We shear[2] the domain $\mathcal{X}_\Phi$ to angle ϕ so that a streak is given by its column position j and two end-points $i_{1,2}$ in that column (Sara and Cvrcek, 2017).[3] Then the streak parameters are $\theta^+ = (\phi, j, i_{1,2})$ which defines its (sheared) domain $\mathcal{Y}(\phi, j, i_{1,2})$. For the sake of brevity, we assume that enumerating $(\phi, j, i) \in \mathcal{Y}(\theta^+)$ is equivalent to enumerating $(\phi, j, i_{1,2}) \in \mathcal{Y}(\phi, j, i_{1,2})$.

We define the distribution that a particular stack in

[2]The shear mapping is two times faster than a rotation.

[3]After shearing the input image to angle ϕ a streak of orientation ϕ becomes vertical, hence simpler to detect by just searching image columns (Tagawa et al., 2016).

the X_Φ contains a single streak with parameters θ^+

$$\hat{p}_1(X_\phi \mid \theta^+) = \hat{p}_0(X_\phi) \prod_{(\phi,i,j)\in\mathcal{Y}(\theta^+)} \frac{p_1(x_{\phi,i,j};\zeta_1(\phi))}{p_b(x_{\phi,i,j};\zeta_b(\phi)}\,, \tag{5}$$

that is analogous to (2). We define the distribution that the image contains a single streak given parameters θ^+ as

$$\hat{p}_1(X_\Phi \mid \theta^+) = \hat{p}_0(X_{\Phi\setminus\phi})\hat{p}_1(X_\phi \mid \theta^+) \tag{6}$$

that is analogous to (3).

Then, we construct the joint distribution, given ϕ

$$\hat{p}_1(X_\phi, j, i_{1,2} \mid \phi) = \\ \hat{p}_1(X_\phi \mid \phi, j, i_{1,2})\,\hat{p}_1(i_{1,2} \mid \phi, j)\,\hat{p}_1(j \mid \phi)\,. \tag{7}$$

We use uniformly distributed priors $\hat{p}_1(i_{1,2} \mid \phi, j)$ and $\hat{p}_1(j \mid \phi)$.

2.3 Certification

We compute the single streak evidence (given orientation) from the model by marginalizing the streak parameters

$$\hat{p}_1(X_\phi \mid \phi) = \sum_{j=1}^{n_\phi} \sum_{i_1=1}^{m_\phi} \sum_{i_2=i_1}^{m_\phi} \hat{p}_1(X_\phi, j, i_{1,2} \mid \phi)\,. \tag{8}$$

Where n_ϕ is number of columns in the sheared image and m_ϕ is the number of rows.

The inner two sums in (8) are easily computed with the help of integral sums, using parametrization $(\phi, j, i_{1,2})$ in the sheared domain and following the Belmann principle of dynamic programming, as in (Sara and Cvrcek, 2017).

We obtain the distribution for complete 3D stack

$$\hat{p}_1(X_\Phi \mid \phi) = \hat{p}_0(X_{\Phi\setminus\phi})\hat{p}_1(X_\phi \mid \phi)\,. \tag{9}$$

Then the full Bayesian evidence required for certification is

$$\hat{p}_1(X_\Phi) = \sum_{\phi\in\Phi} \hat{p}_1(X_\Phi \mid \phi)\,\hat{p}_1(\phi)\,. \tag{10}$$

Where $\hat{p}_1(\phi)$ is a uniform distribution.

We can effectively precompute the partial elements in (9) up to some constant background distribution per individual level in 3D stack.

We have chosen the background distribution to be parameterless and already have the required form $\hat{p}_0(X_\Phi)$.

Certifying streak detection requires statistical decision about the presence of a single streak in the image. We implement the decision as the Bayesian model selection based on the evidences (10) and (3).

The Bayes model selection tells us that an image contains a streak if and only if $\hat{p}_1(X_\Phi) > \hat{p}_0(X_\Phi)$. In practice, we study their ratio

$$C(X) = \frac{\hat{p}_1(X_\Phi)}{\hat{p}_0(X_\Phi)} = \sum_{\phi\in\Phi} \frac{\hat{p}_1(X_\phi \mid \phi)\hat{p}_1(\phi)}{\hat{p}_0(X_\phi \mid \phi)}\,, \tag{11}$$

which we call *certification value* and we say that image contains a streak when

$$C(X) > T\,, \tag{12}$$

where the T is a given threshold. The (12) is then *certification decision*. This is equivalent to the decision rule used in (Sara and Cvrcek, 2017). The need for the threshold T arises from an imperfect power of the statistical model to capture reality. The T then serves as a way to balance the false positive/false negative tradeoff.

The complete certification and detection algorithm is summarized in Alg. 1.

2.4 Detection

Detection is a maximization

$$(\theta^+)^* = \operatorname*{argmax}_{(\phi,i,j)\in\mathcal{Y}(\theta^+)} \hat{p}_1(X_\Phi \mid \theta^+)\,, \tag{13}$$

it can therefore be easily computed simultaneously with certification. We simply replace summations in (8) and (10) by maximizations.

For clarity in subsequent text, we introduce the following function

$$(j^*, i^*_{1,2}) = L(\phi) = \operatorname*{argmax}_{j,i_{1,2}} \hat{p}_1(X_\Phi \mid \phi, j, i_{1,2})\,, \tag{14}$$

which selects the best streak segment, given an angle ϕ.

3 EXPERIMENTS

3.1 Certification

Certification is a decision task whose ROC curve is generated by threshold T in (12). We therefore report ROC curves and also AUC statistics. We used the same experimental procedure as in (Sara and Cvrcek, 2017), which we call the MLBI method here. Note that results in (Sara and Cvrcek, 2017) show ROC curves and AUC with a subset of streak orientation angles ignored, as discussed in Sec. 2. Unlike MLBI, here we are testing on the full angular range. This is the reason the MLBI results reported here are worse than those reported in (Sara and Cvrcek, 2017).

The proposed method produces certification values $C(X)$, so does the MLBI method. False positive

Algorithm 1: Streak certification and detection.

Given: Input image X.

Output: Certificate value $C(X)$, streak parameters $(\phi^*, j^*, i^*_{1,2})$.

1. Get a feature representation $\mathbf{f}_{res}$ of the input image using (1).
2. Initiate Φ to $(-90, -85, ..., 85, 90)[^\circ]$:
3. For each angle $\phi \in \Phi$:
   (a) Find response X_ϕ to the template in Fig. 4 rotated by ϕ.
   (b) Shear response X_ϕ by ϕ (streaks become vertical).
   (c) Learn $\zeta_b(\phi)$.
   (d) Compute $\zeta_1(\phi)$ using (4) and $\hat{p}_0(X_\phi \mid \phi)$ from (2).
   (e) Compute $\hat{p}_1(X_\phi \mid \phi)$ from (8).
   (f) Find the best segment $L(\phi)$ in angle ϕ using (14).
   (g) Update Φ by using the branch and bound method.
4. Compute $\hat{p}_0(X_\Phi)$ from (3) and $\hat{p}_1(X_\Phi)$ from (10).
5. Find the maximum ϕ^* of $L(\phi)$ over $\phi \in \Phi$ by fetching results from Step 3f.
6. Given ϕ^* use (14) to get $(j^*, i^*_{1,2})$.
7. $C(X) \leftarrow \hat{p}_1(X_\Phi)/\hat{p}_0(X_\Phi)$.

occurs when $C(X)$ exceeds the certification decision threshold T. False negative occurs in a streak image with the $C(X)$ lower than T.

To the best of our knowledge, there is no publicly available benchmarking dataset. As a result, different methods are evaluated on different datasets, which are not publicly available. Even the largest published study on the topic (Virtanen et al., 2016) does not publish the dataset. Direct comparison with most of other methods is therefore impossible. In order to compare our results with the closest work, we used a dataset very similar to that one that has been used in (Sara and Cvrcek, 2017).

It is difficult to obtain streak images with verified ground-truth. Manual ground-truth verification is not feasible in very faint streaks, since there are many objects of high apparent magnitude that the human eye cannot see. The difficulty may be acknowledged in Fig. 1, which shows an example of a well detectable streak but an untrained human eye can easily miss it. Obtaining a ground-truth dataset would be a major effort in itself.

Therefore, a ground-truth dataset must be simulated. In order to make the simulation realistic, the (Sara and Cvrcek, 2017) used real images as a background and simulated streaks of varying length, position, orientation, and amplitude in them. We use the same method: One hundred real images are selected from the same large dataset, which either do not contain a streak or contain streak(s) which can not be manually confirmed. The images were taken in Lulin observatory in Taiwan (the same data as in (Yanagisawa et al., 2012; Sara and Cvrcek, 2017)). The 50 cm telescope had FOV $1.3^\circ \times 1.3^\circ$, effective size of images is 2049(V)×2047(H), 16 bit monochromatic and 5.9 s exposure time. Approximately 10 000 random synthetic streaks were additively superimposed onto the background images. Their amplitudes a are related to signal-to-background ratio (SBR) by

$$\mathrm{SBR} = 20 \log_{10} \frac{a}{\sigma}, \qquad [\mathrm{dB}] \tag{15}$$

where σ is the standard deviation of the background values (upper half-percentile is clipped). This is equivalent to SBR defined in (Sara and Cvrcek, 2017). The lower the SBR value the fainter the streak. The streaks were generated so that the distribution of their end points was uniform over the image domain and their SBRs have uniform distribution (SBR $\sim \mathcal{U}(-30, 0)[\mathrm{dB}]$) in the dataset.

We prototyped Algorithm 1 in MATLAB. The processing time was measured on a middle-range laptop with Intel processor i5-6200U CPU @ 2.30GHz ×4. The processing time of an input image is determined by the SBR of a streak in the input image. The method takes up to several (3-7) minutes for streak-less images. If the image contains a streak with higher SBR the processing times decreases to a few (2-4) minutes.

3.2 Certification and Detection Consistency

Detection is done over identical data as certification. We need to evaluate the accuracy of detection, given the ground truth data. The metric determining distance between a detected streak and ground truth is problem dependent. From a practical point of view, the most important parameter of a detection is its orientation angle ϕ. A somewhat less important parameter is the orthogonal distance of detected streak from its correct position (corresponding approximately to j). The least important parameters are the streak endpoints (corresponding to $i_{1,2}$).

For the purpose of this experiment, we chose to measure the angular error between detected and ground truth streak as

$$d(L_{\mathrm{det}}, L_{\mathrm{gt}}) = |\phi_{\mathrm{det}} - \phi_{\mathrm{gt}}|, \tag{16}$$

where ϕ_{det} and ϕ_{gt} is the orientation of the detected streak and the ground truth streak, respectively.

We want to show that certification is consistent with detection accuracy. For each simulated image I, we perform certification followed by streak detection. We retain details about the simulation: The streak

length, orientation and signal to background ratio. In the results section, we study the relation between certification value $C(X)$ and detection. We would like to see that the certification value $C(X)$ is related to streak length and to SBR and that there exist a narrow interval for the certification threshold T which predicts streak detection failure, as measured by the accuracy metric.

4 RESULTS AND DISCUSSION

4.1 Certification

Similarly as in (Sara and Cvrcek, 2017) we split the dataset to several sub-groups based on the streak's SBR and length. As discussed above, short streaks and/or streaks of low SBR are more difficult to certify (and detect).

The results of ROC analysis (Fawcett, 2006) are shown in Figs. 7, 8, 9 and 10. Figs. 8 and 10 show ROC curves of the proposed method. Figs. 7 and 9 show ROC analysis of the MLBI method presented in (Sara and Cvrcek, 2017), this time with no orientation restriction. Each point in Figs. 9 and 10 shows AUC for the given subset. Since we do not restrict the angular space as in (Sara and Cvrcek, 2017), the method in Figs. 7 and 9 show degraded results compared to those reported in (Sara and Cvrcek, 2017).

As can be expected, long, sufficiently bright streaks are easy to certify. In Fig. 10 we see that in the interval of $-10\,\mathrm{dB}$ to $-5\,\mathrm{dB}$, with the shortest streaks, the AUC is 0.925. This means the error rate (Fawcett, 2006) is 7.5%. That is a 6-fold improvement over the MLBI. For the long ($\Delta > 1200$), ultra-faint (SBR $< -25\,\mathrm{dB}$) streaks in Fig. 10 the error rate is still less than 32 %. In this range the MLBI method gives results not better than a chance (AUC ≈ 0.5). We conclude the proposed method significantly exceeds the MLBI method in performance when applied to the full streak orientation domain.

4.2 Certification and Detection Consistency

Certification works well when it is consistent with detection: Only correctly detected streaks should be certified positively.

Box plots in Fig. 11 show dependency of angular error on the SBR for all detections. We see in Fig. 12 that the error is significantly smaller in certified streaks. Even very faint streaks in the $(-30, -20)$ dB range achieve low median detection error.

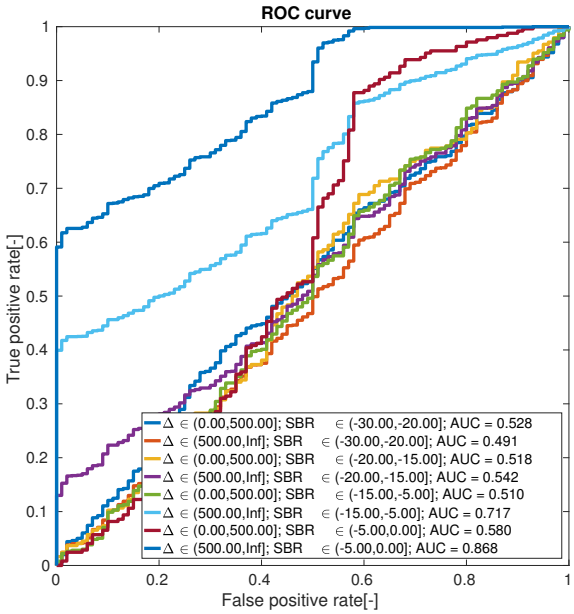

Figure 7: ROC curves for the MLBI method (Sara and Cvrcek, 2017) on the full angular domain. Colors represent dataset subgroups (see the main text for a description) from a Cartesian product listed in the plot legends.

Table 1: Confusion matrix for real streaks, the certification threshold is $\log(C(X)) > 200$.

		Ground truth	
		Streak	Background
Certification	Streak	24 (TP)	4 (FP)
	Backgr.	0 (FN)	18 (TN)

To probe further, the scatter plot in Fig. 13 shows the dependency between the angular error and certificate value $C(X)$. We can see that almost all failed detections occur under $\log C(X) < 200$. The red line shows medians of data groups with a similar certification value. The sharp drop in that curve confirms a stable decision threshold $T \approx 200$ on $\log C(X)$.

4.3 Real Data Experiments

We manually selected 24 observations that contain a streak and 22 observation that do not contain a streak. An example of faint detected streak is in Fig. 14. We run the detection and certification for these observations. The resulting confusion matrix is in Tab. 1.

False negative occurs when the streak is too faint/short. Streaks visible to human are almost always detectable, hence the false negative count is

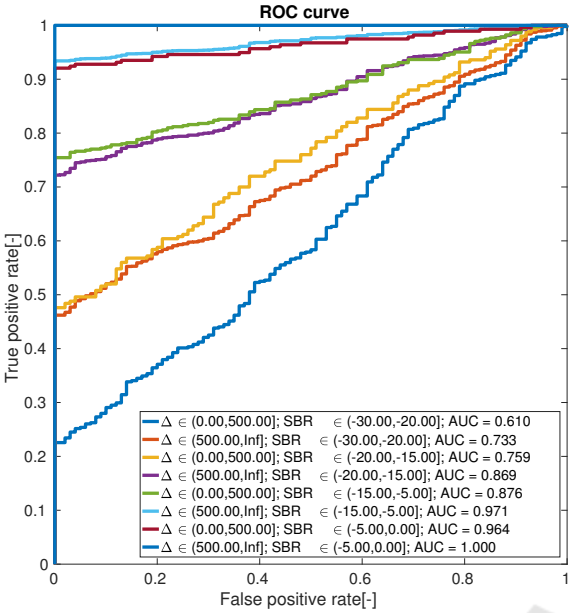

Figure 8: ROC curves for the proposed method, on the full angular domain. Note the marked improvement over Fig. 7 on same-color curves.

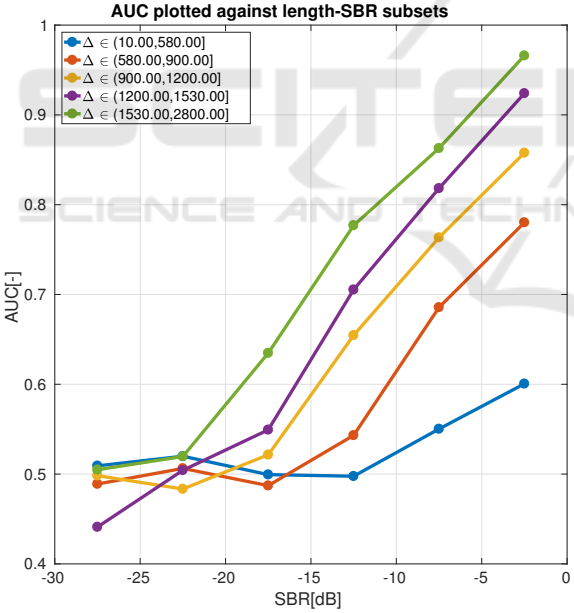

Figure 9: AUC for the MLBI method (Sara and Cvrcek, 2017) on the full angular domain. Colors correspond to streak length intervals, the SBR coordinate represents the middle of a SBR interval.

zero. False positive occurs, when the data are oversaturated (Fig. 15) or the catalog fails (Figs. 16 and 17). Catalog fails, when the star in the catalog is either significantly brighter (Fig. 16) or significantly fainter (Fig. 17). Both instances produce a contrast that leads to a false positive.

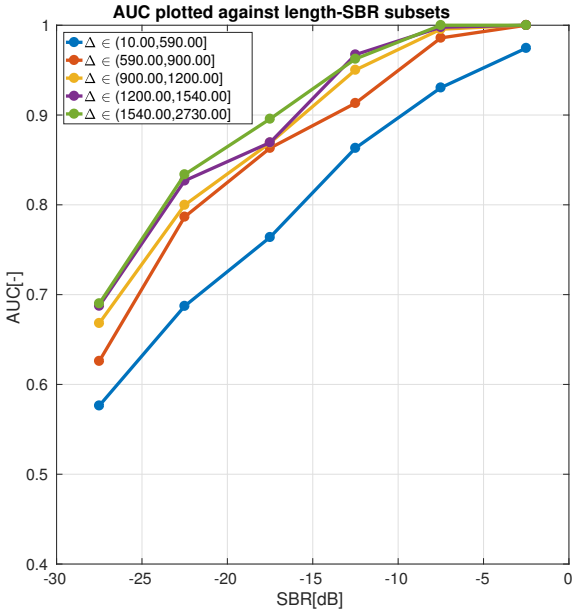

Figure 10: AUC for the proposed method, on the full angular domain. Note the improvement over Fig. 9.

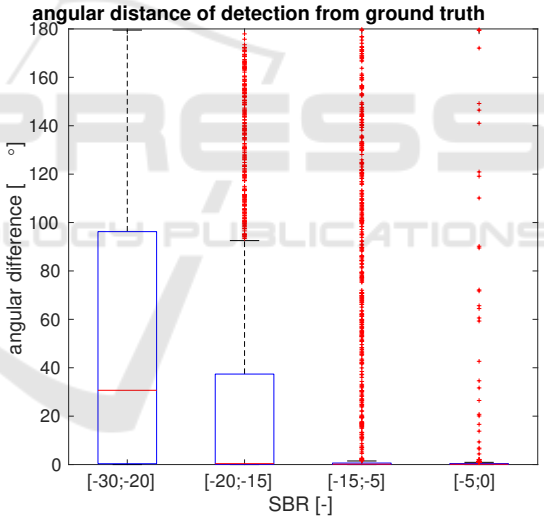

Figure 11: Angular error vs. SBR for all detections. Blue boxes show data from 25th to 75th percentile, red lines are medians.

4.4 Comparison with other Methods

Comparison with other independent methods can only be done indirectly. The (Dawson et al., 2016) demonstrate their method on what they call *ultra-faint streaks*. Their streak has amplitude lower than SBR ($a <$ RMS noise) and length $\Delta \approx 250$ px. This means authors are capable of detecting a streak with SBR lower than 0 dB. The lowest SBR we found in literature is SBR ≈ -4.4 dB (amplitude $\approx 0.6\sigma$ (Zimmer et al., 2013; Schildknecht et al., 2015)). The method

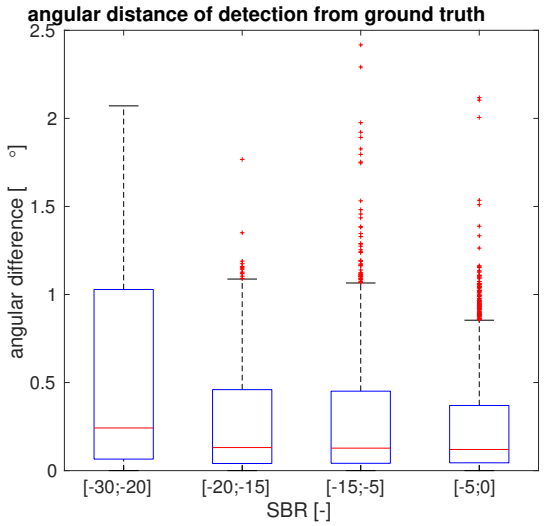

Figure 12: Angular error vs. SBR for detections certified with the threshold of $\log(C(X)) > 200$. Blue boxes show data from 25th to 75th percentile, red lines are medians. Note the scale change on the y axis.

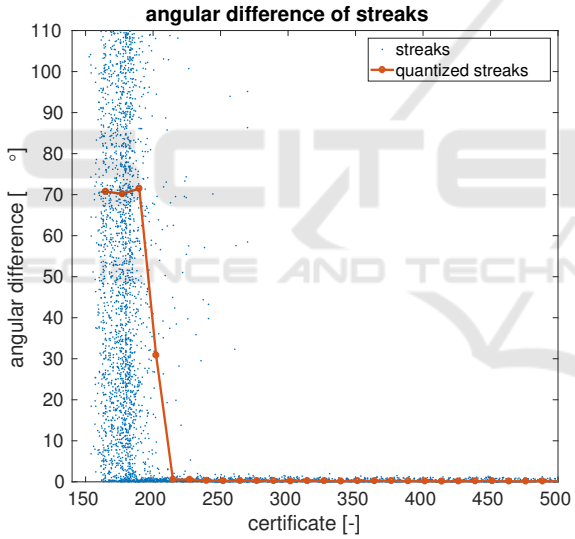

Figure 13: Angular error d as a function of certification value $\log C(X)$. One blue point corresponds to one image.

(Virtanen et al., 2016) is capable of detecting multiple streaks in about 13 s in 2k-by-2k images. The true positives are about 90% for SBR > 0 dB for streaks longer than 100 px. And when the SBR is lower than -6 dB, the true positives are around 50%.

5 CONCLUSION

We have discussed a certification method, which statistically decides about the presence of a streak in the image. We have also shown that background simulation (stars, some sensor artefacts) leads to superior certification results, as demonstrated on semi-synthetic data. We have shown that the certification value predicts detection failure in the sense of a detection error metric.

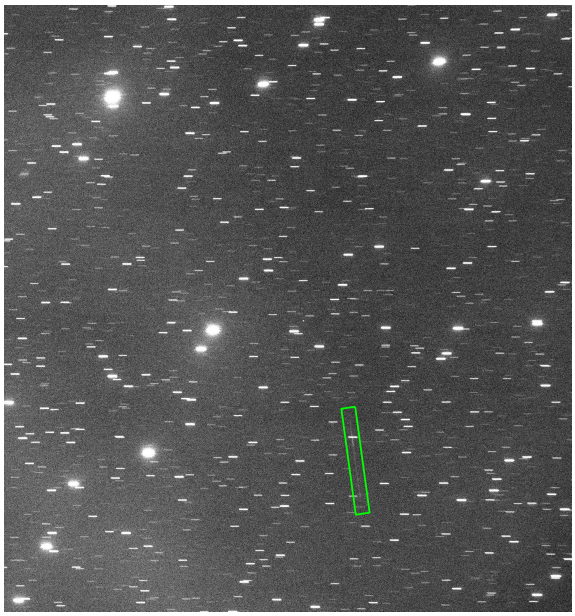

Figure 14: Detection of a real faint streak, the certification value is -325.

We conducted experiments showing that on the SBR interval of -5 dB to 0 dB, with streaks length from 10 px to 500 px, we achieve AUC ≈ 0.97. This is comparable to results presented in (Sara and Cvrcek, 2017). However, unlike in (Sara and Cvrcek, 2017) we can certify a streak regardless of its orientation. The proposed method outperforms (Sara and Cvrcek, 2017) in lower SBRs. Fig. 10 shows that even for the SBR values from -30 dB to -25 dB the error rate of the proposed method is still better than random guessing (AUC > 0.5). Of the known methods this is the best performance.

We also tested the method on a small set of real data in Sec. 4.3. We have shown that the method is capable to detect faint streaks in real datasets. We have also shown that the method often fails when the background compensation fails. This observation hints toward further improvements.

The streak detection domain provides an example of a problem, where the objects of interest are arbitrarily difficult to confirm. We have shown that it is possible to construct a general mechanism that can certify a detection while adapting to the input data instance via constructing the p_b distribution. The generality of the approach follows from the generality of Bayesian inference. The nice property of the st-

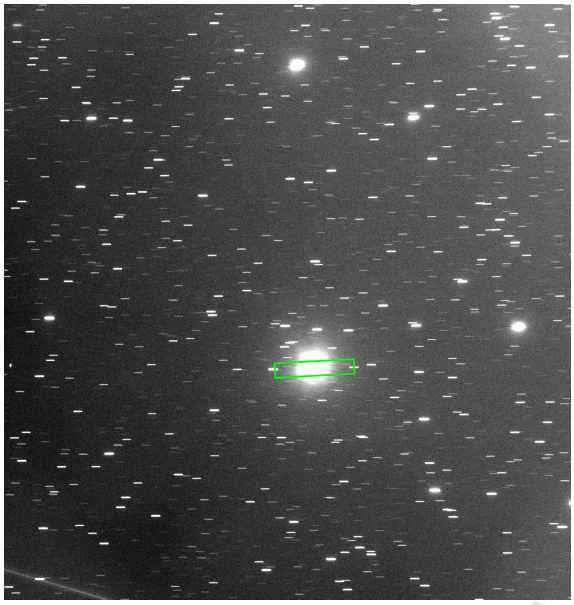

Figure 15: Detection fails because of the large saturated star.

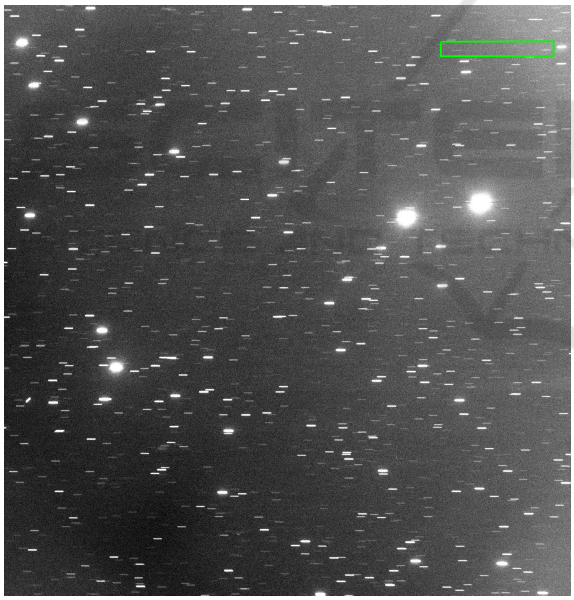

Figure 16: Detection fails because the star in the catalog is too bright. The star is therefore overcompensated and resulting contrast is detected as a streak. Best viewed close-up, in PDF.

reak detection problem is that the marginals needed for the inference can be computed *exactly*. It is therefore possible to study the utility of the Bayesian model selection principle in computer vision problems. Our results confirmed our (good) expectations.

Generalization to multiple streak certification is possible within the model selection framework. Instead of considering just two models M_0 and M_1,

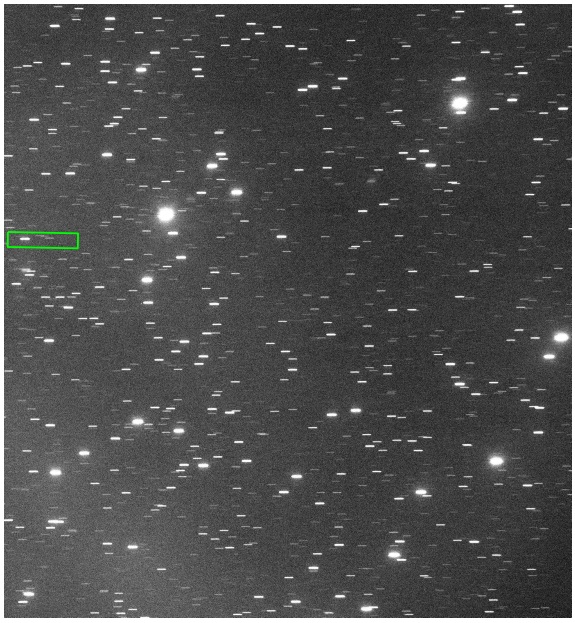

Figure 17: Detection fails because the star in the catalog is too faint. The undercompensated star residual response is similar to a streak.

for no-streak and single-streak data interpretation, respectively, one could consider a set M_i for $i = 0, \ldots, n$. As a result, one would get the a posteriori most probable number of streaks in data. This is a topic for further research.

ACKNOWLEDGMENTS

We acknowledge the support of the CTU Internal grant SGS18/184/OHK3/3T/13 and the OP VVV MEYS funded project CZ.02.1.01/0.0/0.0/16_019/0000765 “Research Center for Informatics”.

Special thanks go to Toshifumi Yanagisawa of JAXA and the TAOS team who made their image data available to us.

REFERENCES

Bobrinsky, N. and Del Monte, L. (2010). The space situational awareness program of the European Space Agency. *Cosmic Research*, 48(5):392–398.

Ciurte, A. and Danescu, R. (2014). Automatic detection of meo satellite streaks from single long exposure astronomic images. In *2014 International Conference on Computer Vision Theory and Applications (VISAPP)*, volume 1, pages 538–544.

Dawson, W., Schneider, M., and Kamath, C. (2016). Blind Detection of Ultra-faint Streaks with a Maximum Li-

kelihood Method. In *Proceedings of the 2016 AMOS Technical Conference*, page 72.

Fawcett, T. (2006). An introduction to ROC analysis. *Pattern Recognition Letters*, 27(8):861 – 874.

Gural, P. S., Larsen, J. A., and Gleason, A. E. (2005). Matched filter processing for asteroid detection. *The Astronomical Journal*, 130(4):1951.

Kolessa, A. E. (2013). Detection of Faint Space Debris Elements with Unknown Orbits. In *6th European Conference on Space Debris*, volume 723 of *ESA Special Publication*, page 143.

Leu, J.-G. (1992). A computer vision process to detect and track space debris using ground-based optical telephoto images. In *Proceedings 11th IAPR International Conference on Pattern Recognition*, pages 522–525.

Marchant, R. and Jackway, P. (2012a). Feature detection from the maximal response to a spherical quadrature filter set. In *Proceedings International Conference on Digital Image Computing Techniques and Applications (DICTA)*, pages 1–8.

Marchant, R. and Jackway, P. T. (2012b). Feature detection from the maximal response to a spherical quadrature filter set. In *DICTA*, pages 1–8.

Sara, R. and Cvrcek, V. (2017). Faint streak detection with certificate by adaptive multi-level Bayesian inference. In *7th European Conference on Space Debris*.

Šára, R., Matoušek, M., and Franc, V. (2013). RANSACing optical image sequences for GEO and near-GEO objects. In *Proceedings of the 2013 AMOS Technical Conference*, page 10.

Schildknecht, T., Schild, K., and Vannanti, A. (2015). Streak detection algorithm for space debris detection on optical images. In *Advanced Maui Optical and Space Surveillance Technologies Conference*, page 36.

Sun, R., Zhan, J., Zhao, C., and Zhang, X. (2015). Algorithms and applications for detecting faint space debris in GEO. *Acta Astronautica*, 110:9 – 17.

Tagawa, M., Yanagisawa, T., Kurosaki, H., Oda, H., and Hanada, T. (2016). Orbital objects detection algorithm using faint streaks. *Advances in Space Research*, 57(4):929 – 937.

Uetsuhara, M. and Ikoma, N. (2014). Faint Debris Detection by Particle Based Track-Before-Detect Method. In *Advanced Maui Optical and Space Surveillance Technologies Conference*.

Virtanen, J., Poikonen, J., Säntti, T., Komulainen, T., Torppa, J., Granvik, M., Muinonen, K., Pentikäinen, H., Martikainen, J., Näränen, J., Lehti, J., and Flohrer, T. (2016). Streak detection and analysis pipeline for space-debris optical images. *Advances in Space Research*, 57(8):1607 – 1623.

Yanagisawa, T. and Kurosaki, H. (2012). Detection of faint GEO objects using JAXA's fast analysis methods. *Transactions of the Japan Society for Aeronautical and Space Sciences, Aerospace Technology Japan*, 10(ists28):29 – 35.

Yanagisawa, T., Kurosaki, H., Banno, H., Kitazawa, Y., Uetsuhara, M., and Hanada, T. (2012). Comparison between four detection algorithms for GEO objects. In *Proceedings of the 2014 AMOS Technical Conference*.

Yanagisawa, T., Kurosaki, H., and Nakajima, A. (2008). The stacking method: The technique to detect small size of GEO debris and asteroids. Technical report, Japan Aerospace Exploration Agency (JAXA).

Yanagisawa, T. and Nakajima, A. (2005). Detection of small LEO debris with line detection method. *Transactions of the Japan Society for Aeronautical and Space Sciences*, 47(158):240–248.

Yanagisawa, T., Nakajima, A., Kadota, K., Kurosaki, H., Nakamura, T., Yoshida, F., Dermawan, B., and Sato, Y. (2005). Automatic detection algorithm for small moving objects. *Publications of the Astronomical Society of Japan*, 57(2):399–408.

Zimmer, P. C., Ackermann, M. R., and McGraw, J. T. (2013). GPU-accelerated faint streak detection for uncued surveillance of LEO. In *Proceedings of the 2013 AMOS Technical Conference*.